ORIGINAL ARTICLE

Contact Mechanism of Rail Grinding with Open-Structured Abrasive Belt Based on Pressure Grinding Plate

Zhiwei Wu[1,2], Wengang Fan[1,2]*, Chang Qian[1,2] and Guangyou Hou[3]

Abstract

The current research of abrasive belt grinding rail mainly focuses on the contact mechanism and structural design. Compared with the closed structure abrasive belt grinding, open-structured abrasive belt grinding has excellent performance in dynamic stability, consistency of grinding quality, extension of grinding mileage and improvement of working efficiency. However, in the contact structure design, the open-structured abrasive belt grinding rail using a profiling pressure grinding plate and the closed structure abrasive belt using the contact wheel are different, and the contact mechanisms of the two are different. In this paper, based on the conformal contact and Hertz theory, the contact mechanism of the pressure grinding plate, abrasive belt and rail is analyzed. Through finite element simulation and static pressure experiment, the contact behavior of pressure grinding plate, abrasive belt and rail under single concentrated force, uniform force and multiple concentrated force was studied, and the distribution characteristics of contact stress on rail surface were observed. The results show that under the same external load, there are three contact areas under the three loading modes. The outer contour of the middle contact area is rectangular, and the inner contour is elliptical. In the contact area at both ends, the stress is extremely small under a single concentrated force, the internal stress is drop-shaped under a uniform force, and the internal stress under multiple concentration forces is elliptical. Compared with the three, the maximum stress is the smallest and the stress distribution is more uniform under multiple concentrated forces. Therefore, the multiple concentrated forces is the best grinding pressure loading mode. The research provides support for the application of rail grinding with open-structured abrasive belt based on pressure grinding plate, such as contact mechanism and grinding pressure mode selection.

Keywords Rail grinding, Abrasive belt, Pressure grinding plate, Contact stress

1 Introduction

Rail grinding is currently recognized as a common means for daily maintenance of rail of various rail transit modes (high-speed rail, heavy load, subway, tram, etc.). By removing rail surface damages, it can effectively improve wheel-rail matching relationship, restrain rolling contact fatigue, extend rail service life, reduce train running noise, improve train running stability and safety, passenger comfort, bring significant social and economic benefits [1–3]. The abrasive belt grinding rail has the advantages of high grinding efficiency, flexible contact, not easy to damage the rail, easy dust recovery, safety and environmental protection, and so on.

Rail grinding with abrasive belt mainly includes closed structures and open structures [4]. The typical structure of open-structured abrasive belt grinding is shown in Figure 1.

*Correspondence:
Wengang Fan
wgfan@bjtu.edu.cn
[1] School of Mechanical, Electronic and Control Engineering, Beijing Jiaotong University, Beijing 100044, China
[2] Key Laboratory of Vehicle Advanced Manufacturing, Measuring and Control Technology, Ministry of Education, Beijing 100044, China
[3] Railway Engineering Research Institute, China Academy of Railway Sciences, Beijing 100081, China

Wu *et al. Chinese Journal of Mechanical Engineering*   (2023) 36:42

Page 2 of 11
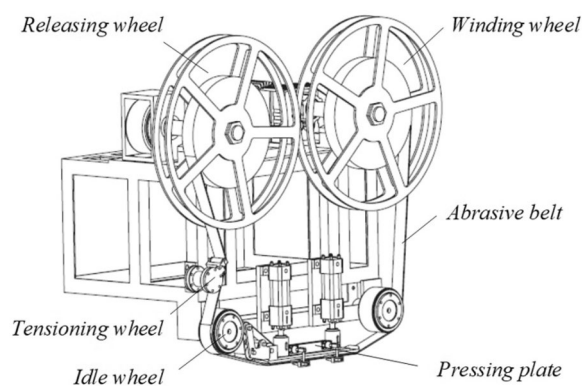
Figure 1 Principle of rail grinding with open-structured abrasive belt based on pressing plate

The rolled abrasive belt is driven by the motor through the winding pulley, so that the abrasive belt can be updated at a constant speed, and the new abrasive belt can always be used to polish the rail, thus ensuring the dynamic stability and quality consistency of the grinding operation. At the same time, the belt-taking mechanism can significantly increase the length of abrasive belt in a single operation, significantly prolong the grinding mileage, avoid frequent replacement of abrasive belt, and greatly improve the grinding efficiency.

The process of rail open abrasive belt grinding is a complex nonlinear interaction among the abrasive belt, the pressure grinding plate and the rail. Studying this complex contact behavior is the theoretical basis for studying the mechanism of material removal. In order to improve the grinding quality and grinding efficiency, it is very important to establish more accurate multi-body contact models and material removal models that conform to actual working conditions.

Blum et al. [5] used the force balance equation and the minimum energy method to regard the contact between the contact wheel and the workpiece as Signorini contact, and established an analytical model for quantitative grinding of abrasive belt. Khellouki et al. [6, 7] studied the contact mechanism between contact wheels with different hardness and cylindrical workpieces when grinding steel rails with open-structure abrasive belts, and established a contact model for qualitative analysis. Deresiewicz et al. [8] regarded the contact relationship between plane contact wheel and workpiece as a simple contact behavior between cylinder and plane, and established the contact wheel friction model. Wang et al. [9] simplified the belt grinding rail with a closed structure to the contact problem between two elastic cylinders based on the elliptic Hertzian contact theory. Wu et al. [10–14] also built a material removal model for precision grinding of

flat contact wheel belt based on Hertz contact theory. Wang et al. [15–17] established the prediction model of abrasive belt wear, grinding power and material removal rate for rail grinding with abrasive belt based on flat contact wheel. Cheng et al. [18–20] established the contact model of rail grinding with closed-structured abrasive belt under static condition by applying elastoplastic theory and Hertz contact theory.

Regarding the research on the open abrasive belt grinding technology, Mohamed et al. [21–23] from the Paris High Tech Engineering School, Rech et al. [24] from the National Engineering School of Saint-Ota, and Jourani et al. [25, 26], conducted a comprehensive study on the formation and wear mechanism of abrasive belts, mainly studied the relationship between the method of characterizing the surface topography of 2D/3D abrasive belts and the degree of surface wear of abrasive belts, and studied in depth the different grinding methods. Influence mechanism of process conditions on abrasive belt wear.

In summary, the existing researches on abrasive belt grinding are mostly closed contact wheel grinding mechanism, experiment and simulation analysis, while the research on contact mechanism of rail grinding with open-structured abrasive belt based on pressure grinding plate is still very scarce. In this research, based on conformal contact and Hertz contact, the contact mechanism of pressure grinding plate, abrasive belt and rail is analyzed. Through finite element simulation and static pressure experiment, the contact behavior of the pressure grinding plate, abrasive belt and rail under the action of single concentrated force, uniform force and multiple concentrated forces is studied, and the distribution characteristics of rail surface contact stress are observed.

2 Contact Analysis for Rail Grinding with Open-Structured Abrasive Belt Based on Pressure Grinding Plate

The research object of this paper is the macroscopic static contact behavior between the pressing plate and the rail contour. The microscale characteristics of the abrasive particles on the surface of abrasive belt and the influence of grinding process on the contact behavior is not taken into account. In the process of grinding, the pneumatic cylinder will press the pressing plate and abrasive belt on the surface of rail, the top surface of pressing plate is applied a concentrated force which is labeled *F*, the concentrated force can be transferred to the curved surface of rail through abrasive belt, so as to remove the material of rail and eliminate the surface damages of rail.

As shown in Figure 2, this paper establishes a coordinate system with the center point of the rail surface as the origin, the tangent plane of the rail surface as the
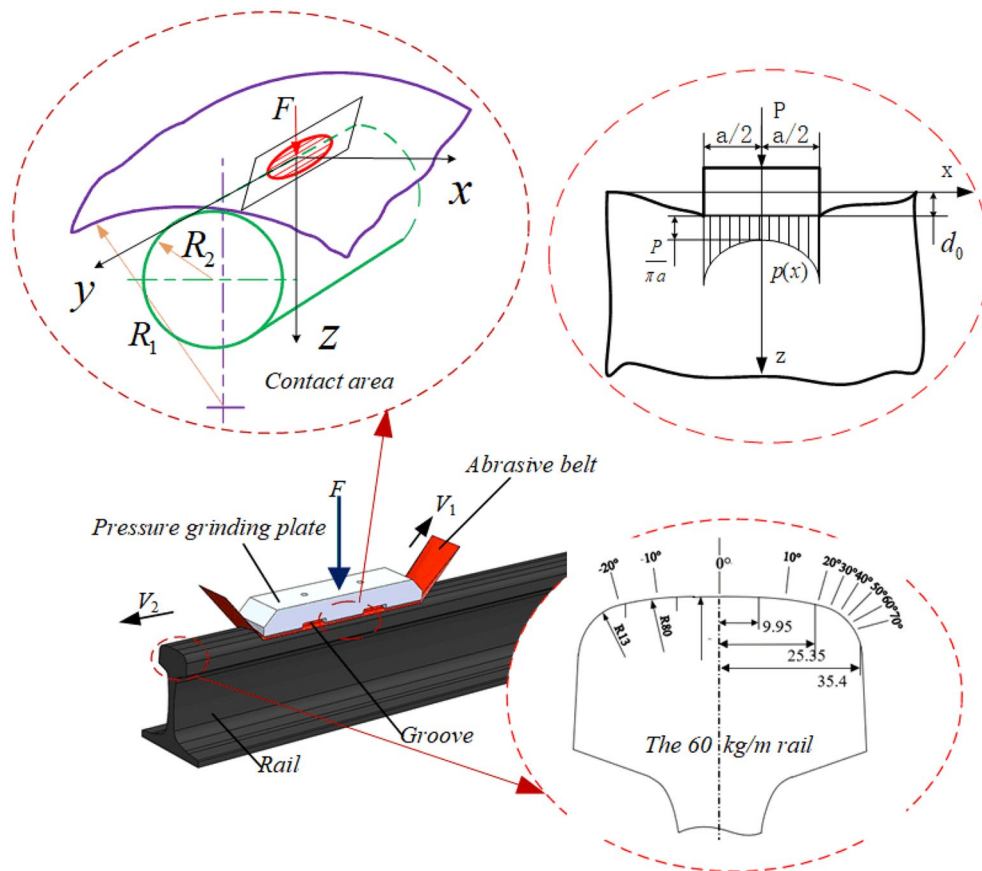
Figure 2 Schematic diagram of press pressing plate—abrasive belt—rail action

XY plane , and the axis perpendicular to the rail surface passing through the origin as the *Z*-axis. Define the direction of the applied force as the positive *Z*-axis.

The rail profile curve is irregular, and it is composed of multiple arcs with different curvatures. Take the 60-standard rail widely used in China as an example. The rail profile is formed by the smooth arcs of R300, R80 and R13, as shown in Figure 2. In order to meet the formation requirements of rail standard profile, the lower surface of the pressing plate is designed as a full-envelope profiling concave curved surface parallel to the rail curvature profile. Thus, the contact among pressure grinding plate, abrasive belt and rail is conformal contact.

For the convenience of analysis, the pressure grinding plate and rail are regarded as two half-planes, and the contact problem is regarded as a problem that an absolutely rigid die acts on an elastic half-plane. According to Ref. [27], the concentrated force acts on the pressure grinding plate, and the contact stress distribution is as shown in Eq. (1):

$$p(x) = \frac{F}{\pi}(a^2 - x^2)^{-1/2}, \quad |x| \le a/2, \; |y| \le l/2, \quad (1)$$

wherein *a* represents the width of pressing plate, *a*=70 mm; *l* represents the length between two slots of the pressure grinding plate, *l*=100 mm.

Therefore, the overall profile of contact stress distribution is rectangular. However, only when a single concentrated force is applied to the center of the pressure grinding plate, the contact center can be regarded as a point contact, that is, the center of the contact area is an elliptical area and the overall outline is rectangular.

According to Hertz theory, as shown in Figure 2, the contact area is an ellipse. According to contact mechanics [28], elastic mechanics [29], Eqs. (2, 3, 4, 5) expresses the size of the ellipse:

$$\frac{1}{E^*} = \frac{1 - v_1^2}{E_1} + \frac{1 - v_2^2}{E_2}, \quad (2)$$

$$\frac{1}{R^*} = \frac{R_1 - R_2}{R_1 R_2}, \tag{3}$$

$$a = \sqrt{\frac{4FR^*}{\pi b E^*}}, \tag{4}$$

$$b = l, \tag{5}$$

wherein E_1, v_1, E_2 and v_2 are the elastic modulus and Poisson's ratio of cylinder 1 and cylinder 2, respectively. R^* and E^* are the effective sphere radius and the effective elastic modulus, respectively.

According to the above formula, the semi-axis lengths a and b of the contact area can be calculated, and then the maximum contact stress can be calculated according to Eq. (6), p_0 is the maximum crushing stress in the contact area:

$$p_0 = \frac{3F}{2\pi ab}. \tag{6}$$

According to the above analysis, the outer contour of the static contact area of the pressing plate, abrasive belt and rail under single concentrated force is rectangular, and the stress concentration area inside is ellipse. However, for the pressing plate, its length is limited, and the external force is concentrated in the center. And rail arc surface is composed of arc segments with different radii. Contact problems are particularly highly non-linear and require significant computer resources to solve. Therefore, the numerical study of pressure distribution in contact area is carried out by the finite element method (FEM), which can accurately combine advanced features into the analysis.

3 Descriptions and Parameters of Numerical Simulation

3.1 Finite Element Model
The contact problem among pressure grinding plate, abrasive belt and rail is a highly nonlinear problem, so this paper chooses ABAQUS software to analyze the contact problem. According to Wang's research [30], in order to promote the heat dissipation of the rail surface and obtain the maximum envelope range, the length of the pressure grinding plate is designed to be 340 mm and the width is designed to be 70 mm. Two grooves are made on the bottom surface of the pressure grinding plate, and the groove width is set to be 30 mm.

The 60 kg/m rail was selected for the rail model. In order to improve the calculation efficiency, save the calculation cost and ensure the accuracy of the results, it is necessary to refine the mesh models of abrasive belt, the upper surface of rail and the lower surface of pressing

Figure 3 Mesh model of sand belt—rail—grinding plate

Table 1 Material parameters

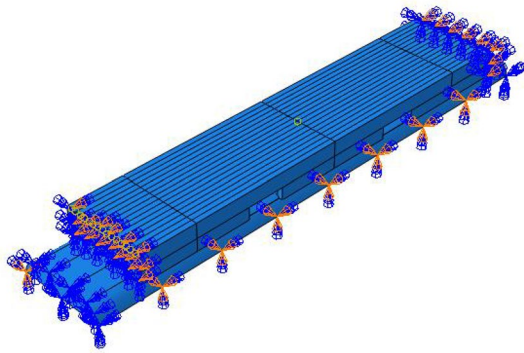| Name	Rail	The abrasive belt	The pressing plate
Elastic modulus (MPa)	2.1×10^5	7.8	2.1×10^5
Density (kg/m³)	7800	2000	7800
Poisson's ratio	0.3	0.47	0.3

plate. In order to avoid malformation or irregularity during meshing, which will affect the simulation accuracy, the thickness of grid cannot be changed suddenly, so the mesh transition strategy is adopted, the mesh model is shown in Figure 3.

The material of 60 kg/m rail is high manganese steel, which is defined as elastic-plastic material. The belt material is a synthetic material, which is defined as an elastic material. The material parameter settings of each model are shown in Table 1.

In order to simulate the actual contact conditions of rail grinding with open-structured abrasive belt based on pressure grinding plate, the boundary conditions of grinding plate, abrasive belt and rail need to be set. Firstly, the contact between the grinding plate and the abrasive belt and the contact between the abrasive belt and the grinding plate are established, respectively. Then define the force application method. Finally, the lower surface of the rail is fixed, and the degrees of freedom of the rail side and the grinding plate rotating along the rail side are constrained. The boundary conditions are set as shown in Figure 4.

3.2 Different Loading Modes
The distribution of contact stress affects the material removal on the rail surface, which directly affects the final rail surface quality. Unreasonable contact stress distribution will lead to poor rail surface quality and affect the stability and safety of train operation. Therefore, the

Wu *et al. Chinese Journal of Mechanical Engineering*   (2023) 36:42

Page 5 of 11

Figure 4 Boundary model of rail –abrasive belt—press grinding plate

(a) Single concentrated force

(b) Uniformly distributed load

(c) Multi-concentration

Figure 5 Different load modes on contact force: **a** Single concentrated force; **b** Uniformly distributed load; **c** Multi-concentration

analysis of different loading modes is very important to study the distribution of contact stress.

When a single concentrated force is used to grind the rail, the applied force is located in the center of the pressure grinding plate, and the direction is vertically downward, as shown in Figure 5(a). The size of a single concentrated force is set from 200 to 1200 N, which is indicated by *F.*

Uniformly distributed load refers to the force or load uniformly distributed on the surface of the object. Under the uniform load, all points on the upper surface of the grinding plate are equally loaded. In order to discuss the distribution of contact stress on rail surface under uniform load, uniformly distributed load is applied to the surface of grinding plate, and other parameters are the same as those of single concentrated force simulation, as shown in Figure 5(b). The uniform load is set from 0.02 to 0.06 N/mm^2, which is indicated by *q.*

Based on the single concentrated force application mode, multiple concentrated force application positions are set. Because of the two grooves in the bottom of the pressure grinding plate, it is divided into three parts. Thus, six symmetrically distributed concentrated forces with the same size are arranged on the surface of the pressure grinding plate. In order to compare the influence of the force application position on the contact stress under the multi-concentration force, the position of the multi-concentration force application point is shown in Figure 6. Among them, the force applying position 1 is closest to the middle position of the pressure grinding plate, and the force applying position 7 is closest to its edge.
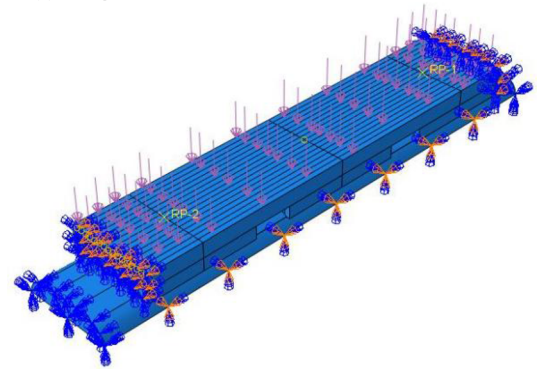
3.3 Results and Discussion
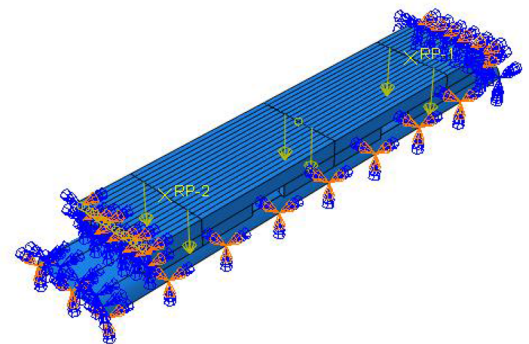
3.3.1 Single Concentrated Force

The nephogram of contact stress under different grinding pressures is shown in Figure 7. The contact stress increases with the increase of grinding pressure, and there is almost no contact stress in the grooved part. The contact stress area is divided into three parts: the outer contour of the middle area is rectangular and the inner contour is elliptical. The contact stress at both ends is triangular and extremely small. Because the stress position is located in the center of the pressure grinding plate and the influence of the rail profile, the contact stress is mainly concentrated in the middle of the rail. The farther
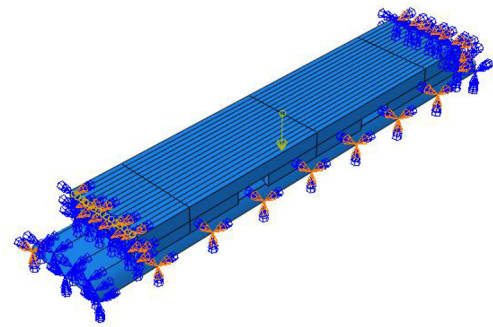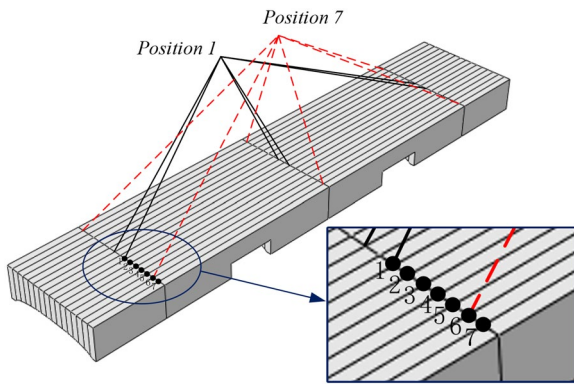
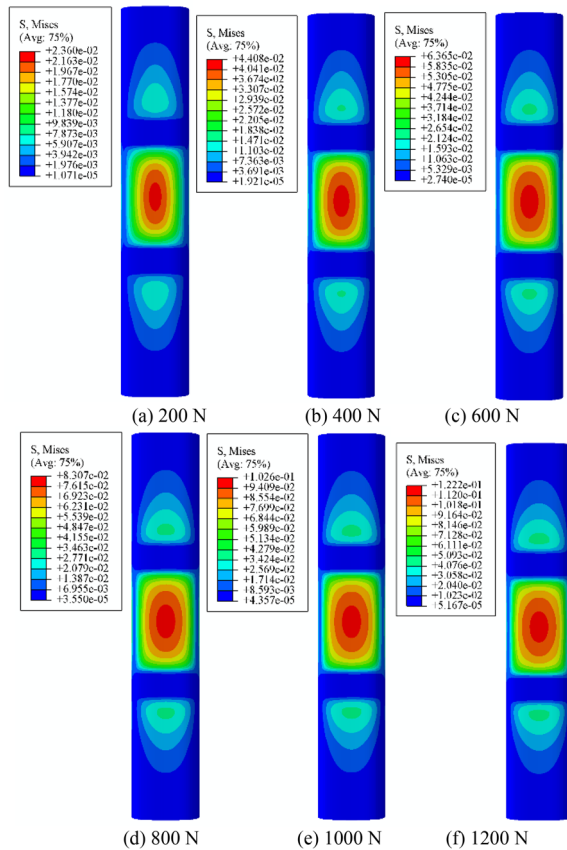**Figure 6** Positions of multiple concentration force application

Figure 7 Stress cloud diagram of single concentrated force: **a** 200 N; **b** 400 N; **c** 600 N; **d** 800 N; **e** 1000 N; **f** 1200 N

Figure 8 Schematic diagram of cross-section and node
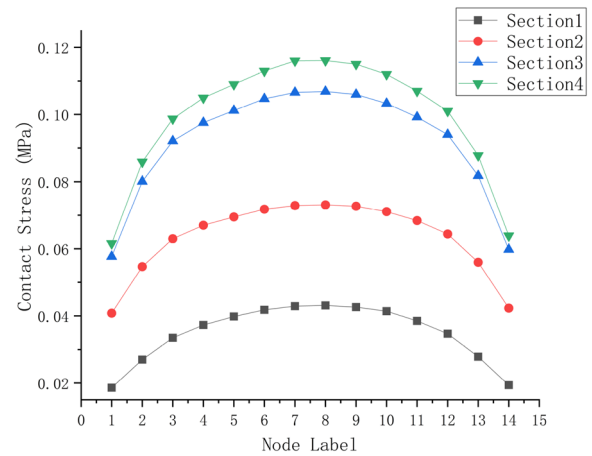
Figure 9 Contact stress nephogram of cross-section under single concentrated force

away from the force application position along the track direction, the smaller the contact stress.

It can be seen from Figure 7 that the contact stress on the rail surface is symmetrical with respect to the middle cross section. In order to more intuitively analyze the surface stress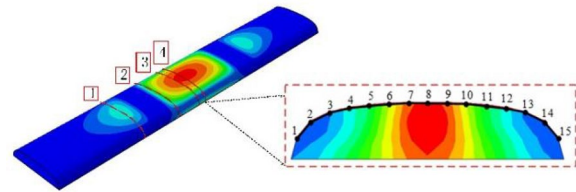 distribution of the rail parallel to the end face of the rail under the action of a single concentrated force, as shown in Figure 8, four sections parallel to the end face of the rail were selected, and the contact stress at 15 points on the section was extracted. Figure 9 shows the contact stress distribution of the four sections under the action of 1200 N concentrated force. The contact stress is concentrated in the middle of the rail, and the contact stress distribution of different sections is similar, but the magnitude is obviously different. The maximum contact stress occurs at the 8th node of the fourth section, and the maximum contact stress is 0.12 MPa.

In addition, in order to better explore the impact of contact under single concentrated force, the corresponding experimental research was carried out in this paper. Figure 10 shows the static pressure experimental system for belt grinding rails based on a pressure grinding plate. The pressure-sensitive paper is double-sheet 4LW film. This device mainly adopts the structure of hand screw, and the rotating handle drives the screw to rotate to apply pressure to the rail. At the same time, the pressure sensor is installed under the rail, and the digital pressure gauge can capture the applied pressure value in real time. During the experiment, the contact area and pressure distribution were recorded by the 4LW pressure film of fujifilm. Then, the pressure film after the experiment is

Wu *et al. Chinese Journal of Mechanical Engineering* (2023) 36:42

Page 7 of 11
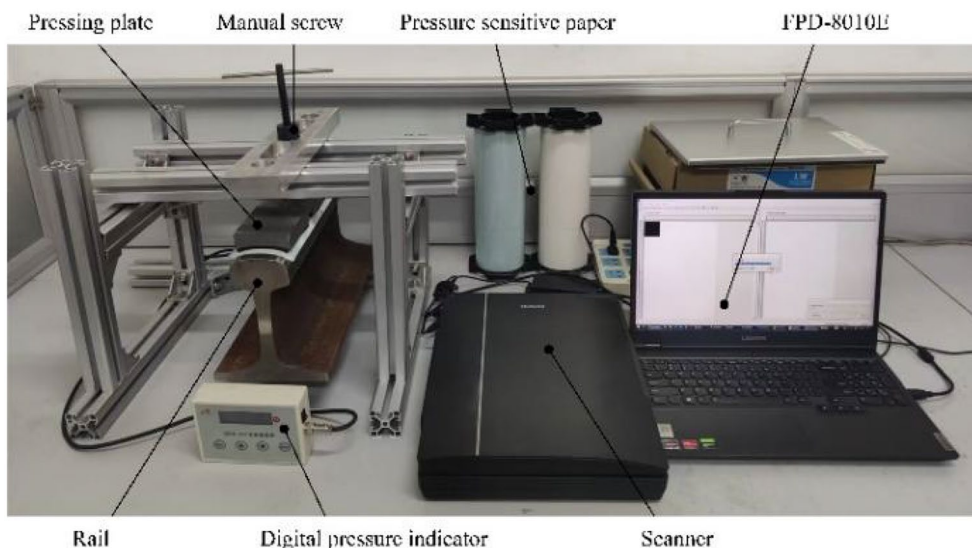
Figure 10 Experimental device for grinding contact between rail, pressing plate and abrasive belt
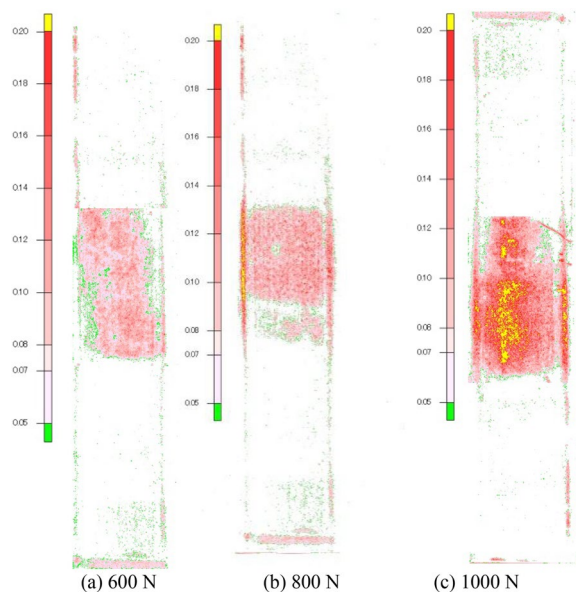
Figure 11 Experimental results of applying single concentrated force: **a** 600 N; **b** 800 N; **c** 1000 N

scanned, and the monochromatic features from the compressed film are converted into point pressure data sets by using the post-processing system FPD-8010E, and the stress gradients obtained from the experiment are indicated in different colors.
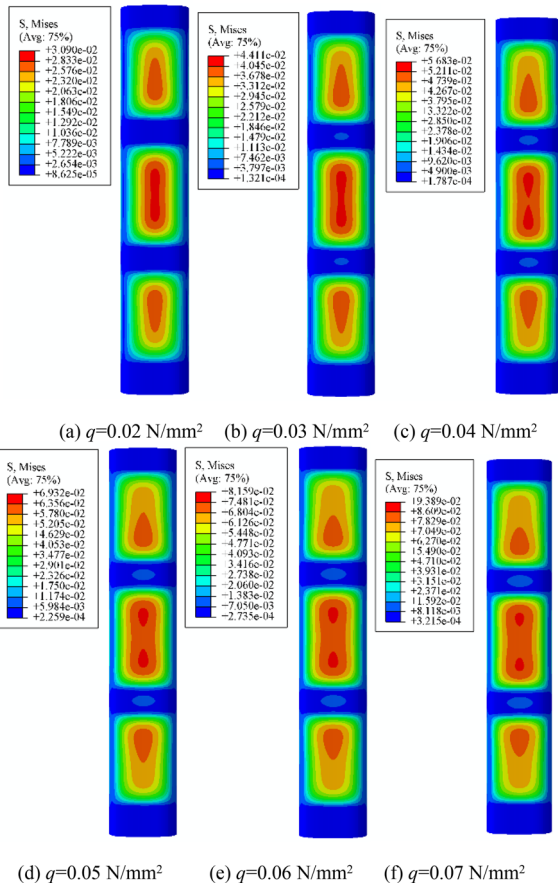
Figure 11 shows the experimental results when a single concentrated force is applied. It can be seen from the figure that the contact stress in the middle of the rail is obvious, and the color changes from deep to shallow from

the center to the periphery. There is almost no stress at both ends of the rail, because when a single concentrated force is applied, the stress at both ends is extremely small, which exceeds the display range of pressure-sensitive adhesive paper.
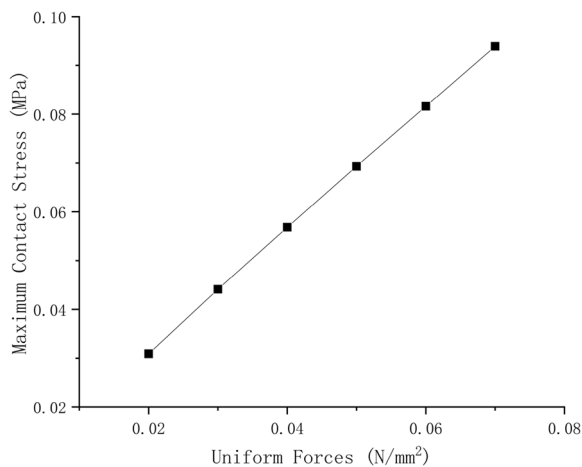
3.3.2 Contact Stress Distribution under Uniform Force

The nephogram of rail surface contact stress under uniform force is shown in Figure 12. The results show that the contact stress on the rail surface is non-uniform and divided into three regions. The shape of the outer contour of the contact area is almost the same, all of which are long strips, because the pressure grinding plate is in conformal contact with the rail. The contact areas are symmetrically distributed about the X axis, and each contact area is internally provided with a drop-shaped place with a large stress and close to the grooved part. The stress distribution in the middle contact area is elliptical. With the increase of uniform load, the larger stress area changes from long strip to water drop near the groove, which is caused by the sudden change of stress at the contact edge of the object.

In order to more clearly analyze the variation law of the contact stress of the rail surface under the uniformly distributed load, the maximum contact stress of the rail surface under the uniformly distributed load is made as shown in Figure 13. The maximum contact stress on the rail surface increases with the increase of the uniform load. The contact stress has a linear positive correlation with the uniformly distributed load, and the ratio of the contact stress to the uniformly distributed load is about 1.32.

Wu *et al. Chinese Journal of Mechanical Engineering*   (2023) 36:42

Page 8 of 11

(a) *q*=0.02 N/mm²   (b) *q*=0.03 N/mm²   (c) *q*=0.04 N/mm²

(d) *q*=0.05 N/mm²   (e) *q*=0.06 N/mm²   (f) *q*=0.07 N/mm²

Figure 12 Distribution of contact stress under uniform forces of different sizes: **a** *q*=0.02 N/mm²; **b** *q*=0.03 N/mm²; **c** *q*=0.04 N/mm²; **d** *q*=0.05 N/mm² ; **e** *q*=0.06 N/mm²; **f** *q*=0.07 N/mm²

In addition, in order to better explore the contact stress distribution under the action of uniform force, corresponding experimental studies are carried out in this paper. Figure 14 shows the experimental results when a uniform force is applied. It can be seen from the figure that the contact stress is divided into three rectangular contact areas, the color of each contact area becomes lighter from the center to the surrounding area, and the color of each contact area near the groove is darker.

3.3.3 Contact Stress Distribution under Multiple Concentrated Force

The nephogram of contact stress distribution under multiple concentrated forces is shown in Figure 15. The results show that the contact stress on the rail surface is non-uniform and divided into three regions. The shape of the outer contour of the contact area is almost the same, all of which are long strips, because the pressure grinding plate is in conformal contact with the rail. With respect to the axial symmetry distribution of the contact area about *X*, the stress concentration parts in the upper and lower contact areas are in the shape of water drops, and the stress concentration areas are far away from the slot position. The stress concentration area in the middle contact area presents an elliptical distribution, and with the concentrated force gradually moving outward, the stress concentration area also increases. With the multi-concentration force position from the center to both ends,

Figure 13 Graph of maximum contact stress with uniformly distributed load

(a) *q*=0.03 N/mm²   (b) *q*=0.05 N/mm²   (c) *q*=0.07 N/mm²
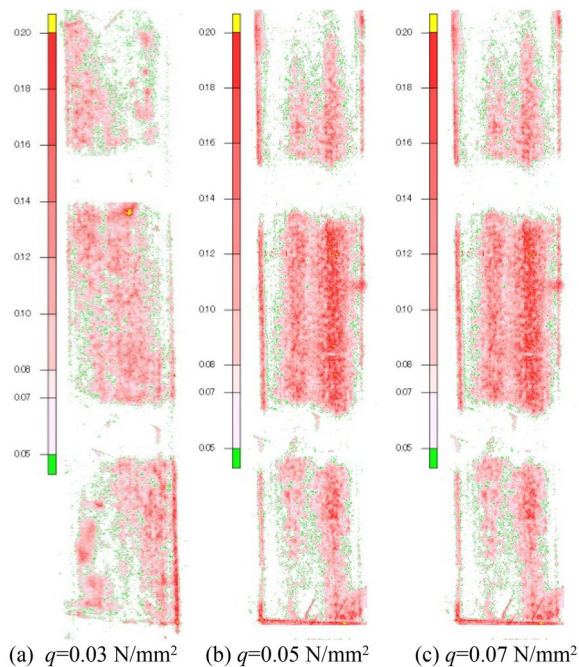
Figure 14 Experimental results of applying uniform force: **a** *q*=0.03 N/mm²; **b** *q*=0.05 N/mm²; **c** *q*=0.07 N/mm²

(a) Force position 1　(b) Force position 2　(c) Force position 3

(d) Force position 4　(e) Force position 5　(f) Force position 6
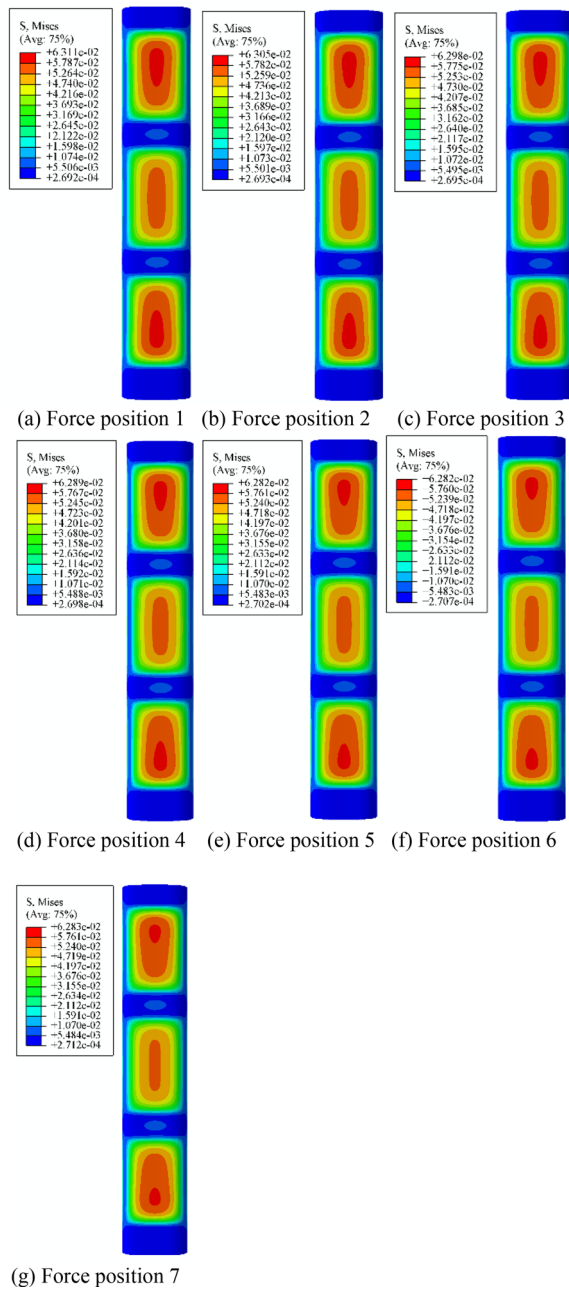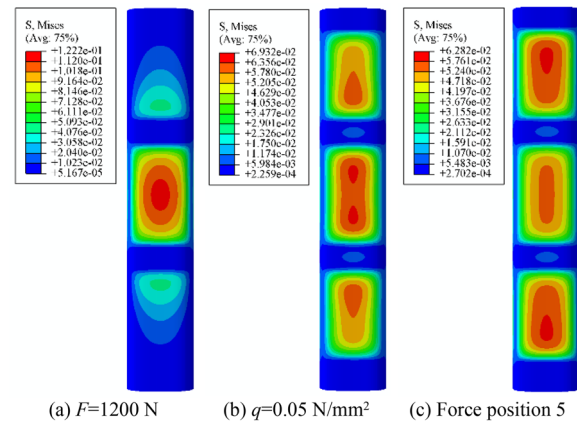

(g) Force position 7

Figure 15 Distribution of contact stress at different force position:
a Force position 1; **b** Force position 2; **c** Force position 3; **d** Force
position 4; **e** Force position 5; **f** Force position 6; **g** Force position 7

the stress distribution becomes more and more uniform, and the maximum stress is basically unchanged.

To sum up, the stress distribution is more uniform when multiple concentrated forces are applied. In addition, considering the possible influence of mechanical devices in actual use, the position cannot be particularly

(a) *F*=1200 N　　(b) *q*=0.05 N/mm²　　(c) Force position 5

Figure 16 Comparison of contact stress under different load modes:
a *F*=1200 N; **b** *q*=0.05 N/mm²; **c** Force position 5

external, so it is more appropriate to select the position No. 5 for the application of multiple concentrated forces.

3.3.4 Comparison of Contact Stress under Different Load Modes

In order to ensure the comparability of the data, the same force is chosen to be applied, corresponding to a single concentrated force of 1200 N, a uniformly distributed force load of $q = 0.05$ N/mm², and a multi-concentrated force of 200 N each. The corresponding simulation diagram is shown in Figure 16. It can be seen from the figure that the stress distribution is the most uniform under the action of multiple concentrated forces. Under the same external force, the maximum contact stress under multi-point concentrated force is the smallest.

4 Conclusions

In this paper, the contact mechanism of rail grinding with open-structured abrasive belt based on pressure grinding plate is studied. It can be concluded that:

(1) Through the conformal contact theory and the Hertz theory, the contact relationship among the pressure grinding plate, the abrasive belt and the rail is analyzed, and it is concluded that the outer contour of the contact area is rectangular, and the inner distribution is elliptical.

(2) There are three contact regions for the contact stress in each loading mode. In the case of a single concentrated force, the contact stress is concentrated in the middle of the rail, and the stress at both ends is extremely small. The outer contour of the contact stress in the middle area is a rectangle, and the inner contour is an ellipse. Under the action of uniform load, the outer contours of the

three contact areas are all rectangular, and there is a drop-shaped stress concentration area inside, which is concentrated on the top of the rail surface. Under the action of multiple concentrated forces, the outer contours of the three contact areas are all rectangular, and the distribution of the inner stress concentration areas is large.

(3) Under the same external load, the multi-concentrated force loading mode is adopted, the contact stress distribution is the most uniform, and the maximum stress is the smallest.

Authors' Contributions
WF was in charge of the whole trial; ZW, CQ and GH wrote the manuscript; ZW and GH assisted with sampling and laboratory analyses. All authors read and approved the final manuscript.

Authors' Information
Zhiwei Wu, born in 1994, is currently a PhD candidate at *Key Laboratory of Vehicle Advanced Manufacturing, Measuring and Control Technology, Ministry of Education, Beijing Jiaotong University, China*. He received his master degree from *North China University of Technology, China*, in 2020.
Wengang Fan, born in 1985, is currently an associate professor at *Beijing Jiaotong University*. He received his PhD degree from *Beijing Jiaotong University, China*, in 2012. His main research direction is rail grinding technology and equipment, digital manufacturing technology and equipment.
Chang Qian, born in 1997, is currently a master candidate at *Key Laboratory of Vehicle Advanced Manufacturing, Measuring and Control Technology, Ministry of Education, Beijing Jiaotong University, China*. She received her master degree from *Beijing Jiaotong University, China*, in 2022.
Guangyou Hou, born in 1994, is currently an engineer at *China Academy of Railway Sciences*. He received his master degree from *Beijing Jiaotong University, China*, in 2020.

Availability of data and materials
The datasets supporting the conclusions of this article are included within the article.

Competing interests
The authors declare no competing financial interests.

References
[1] S D Zhi, J Y Li, A M Zarembski. Grinding motor energy saving method based on material removal model in rail grinding processes. *International Journal of Precision Engineering and Manufacturing-Green Technology*, 2015, 2(1): 21-30.
[2] W Fan, W Wang, J Wang, et al. Microscopic contact pressure and material removal modeling in rail grinding using abrasive belt. *Proceedings of the Institution of Mechanical Engineers, Part B: Journal of Engineering Manufacture*, 2021, 235(1-2): 3-12.
[3] W Wang, J Li, W Fan, et al. A numerical model to investigate contact status for rail grinding by abrasive belt with an axial deflection. *Journal of the Brazilian Society of Mechanical Sciences and Engineering*, 2019, 41(11): 494.
[4] W Fan, J Wang, J Cheng, et al. Dynamic contact modeling considering local material deformation by grit indentation for abrasive belt rail grinding. *The International Journal of Advanced Manufacturing Technology*, 2020, 108(7-8): 2165-2176.
[5] H Blum, F T Suttmeier. An adaptive finite element discretisation for a simplified Signorini problem. *Calcolo*, 2000, 37: 65-77.
[6] A Khellouki, J Rech, H Zahouani. The effect of abrasive grain's wear and contact conditions on surface texture in belt finishing. *Wear*, 2007, 263(1-6): 81-87.
[7] A Khellouki, J Rech, H Zahouani. Influence of the belt-finishing process on the surface texture obtained by hard turning. *Proceedings of the Institution of Mechanical Engineers Part B: Journal of Engineering Manufacture*, 2007, 22l(7): 1129-1137.
[8] S Mezghani, M E Mansori, H Zahouani. New criterion of grain size choice for optimal surface texture and tolerance in belt finishing production. *Wear*, 2008, 266: 578-580.
[9] R Q Wang. *The modeling and experimental research of belt grinding process in rail*. Beijing: Beijing Jiaotong University, 2016. (in Chinese)
[10] C L Wu, H Y Ding, Y Chen. Research on modeling method of material removal depth in CNC mechanical polishing for aluminum alloy wheel. *China Mechanical Engineering*, 2009, 20(21): 2558-2562. (in Chinese)
[11] C L Wu, H Y Ding, Y Chen. Research on modeling method of relation between abrasive grain and material removal depth. *China Mechanical Engineering*, 2011, 22(3): 300-304. (in Chinese)
[12] W Wang, F Liu, Z Liu, et al. Prediction of depth of cut for robotic belt grinding. *International Journal of Advanced Manufacturing Technology*, 2017, 91(1-4): 699-708.
[13] G Xia, Y Huang. Adaptive belt precision grinding for the weak rigidity deformation of blisk leading and trailing edge. *Advances in Mechanical Engineering*, 2017, 9(10): 1-12.
[14] Y Wang, Y Huang, Y Chen, et al. Model of an abrasive belt grinding surface removal contour and its application. *International Journal of Advanced Manufacturing Technology*, 2016, 82(9-12): 2113-2122.
[15] W X Wang, J Y Li, W G Fan, et al. Abrasion process modeling of abrasive belt grinding in rail maintenance. *Journal of Southwest Jiaotong University*, 2017, 52(1): 141-147.
[16] W X Wang, J Y Li, W G Fan, et al. Grinding power prediction model for abrasive belt rail grinding based on Hertzian contact. *China Railway Science*, 2017, 38(3): 25-30.
[17] W G Fan, Y M Liu, W X Wang, et al. Research on modeling method of material removal for rail grinding by abrasive belt based on elastic Hertzian contact. *Journal of Mechanical Engineering,* 2018, 54(15): 191-198. (in Chinese)
[18] W G Fan, J F Cheng, H B Lü, et al. Research on time-varying contact behavior and simulation for waved rail surface grinding by abrasive belt. *Journal of Mechanical Engineering*, 2018, 54(4): 87-92. (in Chinese)
[19] W G Fan, J F Cheng, Y F Wu, et al. Research on static contact behavior and simulation for rail grinding by abrasive belt based on concave type contact wheel. *Journal of Mechanical Engineering*, 2018, 54(14): 152-158. (in Chinese)
[20] J J Roseman. The principle of Saint-Venant in linear and non-linear plane elasticity. *Archive for Rational Mechanics and Analysis*, 1967, 26(2).
[21] M E Mansori, E Sura, P Ghidossi, et al. Toward physical description of form and finish performance in dry belt finishing process by a tribo-energetic approach. *Journal of Materials Processing Technology*, 2007, 182(1-3): 498-511.
[22] S Mezghani, M E Mansori. Abrasiveness properties assessment of coated abrasives for precision belt grinding. *Surface & Coatings Technology*, 2008, 203(5-7): 786-789.
[23] K Serpin, S Mezghani, M Mansori. Wear study of structured coated belts in advanced abrasive belt finishing. *Surface & Coatings Technology*, 2015, 284: 365-376.
[24] A Khellouki, J Rech, H Zahouani. The effect of lubrication conditions on belt finishing. *International Journal of Machine Tools & Manufacture*, 2010, 50(10): 917-921.

[25] A Jourani, B Hagège, S Bouvier, et al. Influence of abrasive grain geometry on friction coefficient and wear rate in belt finishing. *Tribology International*, 2013, 59.

[26] A Jourani, M Dursapt, H Hamdi, et al. Effect of the belt grinding on the surface texture: Modeling of the contact and abrasive wear. *Wear*, 2005(2): 259.

[27] X A Kong, X Y Jiang, X S Jin, et al. *Solid contact mechanics*. Beijing: China Railway Publishing House Co., LTD., 1999. (in Chinese)

[28] L P Valentin. Contact mechanics and friction physical principles and applications. *Tribology Letters*, 2010, 40(3).

[29] L D Landau, E M Lifschitz. *Theory of elasticity (Theoretical Physics, Vol. 7)*. 3rd ed. Butterworth-Heineemann, Oxford, 1999: 8-9.

[30] H Wang. *Simulation and analysis of active chip eliminate process using open-structured abrasive belt for rail grinding*. Beijing: Beijing Jiaotong University, 2019. (in Chinese)